

**Univerzita Karlova**  
**Přírodovědecká fakulta**

Studijní program: Chemie

Studijní obor: Chemie



**Adam Škorňa**

Asociační chování hvězdicových kopolymerů s amfifilními rameny

Association behavior of star copolymers with amphiphilic arms

Bakalářská práce

Školitel: doc. RNDr. Miroslav Štěpánek. Ph.D.

Praha 2020/2021

## **Prohlášení:**

Prohlašuji, že jsem závěrečnou práci zpracoval/a samostatně a že jsem uvedl/a všechny použité informační zdroje a literaturu. Tato práce ani její podstatná část nebyla předložena k získání jiného nebo stejného akademického titulu.

V Praze, 16.06.2021

Podpis

## Abstrakt

Bakalářská práce se zabývá asociativním chováním dvou amfifilních hvězdicových polymerů, složených z 41, resp. 29 hydrofilních ramen poly(2-(*N,N*-dimethylamino)ethyl methakrylát) u (PDMAEMA, molekulová hmotnost ramene 6,0 kg mol<sup>-1</sup>) a 26, resp. 88 hydrofobních ramen poly(lauryl methakrylát) u (PLMA, molekulová hmotnost ramene 4,6 kg mol<sup>-1</sup>) ve vodných roztocích, pomocí statického a dynamického rozptylu světla a transmisní elektronové mikroskopie. Vzhledem k tomu, že polymery nebyly přímo rozpustné ve vodě, byl jako kosolvent použit tetrahydrofuran, který je dobrým rozpouštědlem ramen PLMA, a po rozpuštění odstraněn dialýzou, takže takto připravené polymerní částice byly v kineticky zamrzlém stavu. Bylo zjištěno, že postup přípravy měl značný vliv na velikost a molekulovou hmotnost polymerních částic. Charakterizace ukázala, že v případě polymeru s vyšším obsahem PLMA (88 ramen) vznikaly, místo micel s jádrem tvořeným PLMA a korónou tvořenou PDMAEMA, nanoprecipitované agregáty.

## **Abstract**

The Thesis deals with association behaviour of two amphiphilic miktoarm star copolymers composed of 41 (or 29) hydrophilic arms of poly(2-(*N,N*-dimethylamino)ethyl methacrylate) (PDMAEMA, molar mass of the arm  $6.0 \text{ kg mol}^{-1}$ ) and 26 (or 88) hydrophobic arms of poly(lauryl methacrylate) (PLMA, molar mass of the arm  $4.8 \text{ kg mol}^{-1}$ ) arms in aqueous solutions, using a combination of static and dynamic light scattering and transmission electron microscopy. Since the polymers were not directly soluble in water, tetrahydrofuran as a good solvent for PLMA was used as cosolvent and after dissolution of the sample it was removed by dialysis, thus leaving formed star polymer nanoparticles in a kinetically frozen state. It was found that both size and molar mass of particles were strongly dependent on the used preparation protocol. Characterization showed that in the case of the PDMAEMA-PLMA sample with a higher PLMA content (88 PLMA arms), the polymer formed nanoprecipitated aggregates instead of micelles with a PLMA core and PDMAEMA corona.

## **Abbreviations**

BCPs – Block copolymers

CMC – Critical micellization concentration

SLS – Static light scattering

DLS – Dynamic light scattering

THF – Tetrahydrofurane

Saf – Star arm-first

PDMAEMA – poly(2-(N,N-dimethylamino)ethyl methacrylate)

PLMA – poly(lauryl methacrylate)

PFF – Particle from factor

PE – Polyelectrolyte

EMG - Electromagnetic

APD – Avalanche photodiode

# Content

<b>1. Introduction</b> .....	1
<b>2. Overview of literature</b> .....	3
2.1. Block copolymers.....	3
2.2. Molecular architectures of BCPs.....	3
2.3. Star-shaped block copolymers.....	4
2.4. Living polymerisations of star-shaped macromolecules.....	5
2.5. Self-assembly of star-shaped block copolymers .....	6
2.6. Properties of BCP in solutions .....	7
2.7. PDMAEMA- <i>b</i> -PLMA copolymers .....	8
2.8. Light scattering.....	9
2.9. Transmission electron microscopy.....	13
<b>3. Materials and methods</b> .....	14
3.1. Polymer samples.....	14
3.2. Preparation methods.....	14
3.3. Photometer.....	15
3.4. Transmission electron microscope .....	15
<b>4. Results and discussion</b> .....	16
<b>5. Conclusion</b> .....	22
<b>6. References</b> .....	22

# 1. Introduction

Block copolymers (BCs) are an interesting group of macromolecular substances with the ability to form self-assembled nanostructures both in melt and in solution, as a result of mutual incompatibility of constituent homopolymer blocks. Such nanostructures find applications in many fields from material engineering and electronics to medicine and pharmacology. Not surprisingly, BCs have been a subject of keen interest of researchers for decades.

Considering biomedical applications, so-called amphiphilic BCPs abilities to form self-assembled nanoparticles (micelles, vesicles) in aqueous media are of special importance. As water is often too strong a precipitant for the hydrophobic block, amphiphilic BCPs are usually not directly soluble in water (unless the hydrophobic block is very short) and their aqueous solutions have to be prepared indirectly using a water-miscible cosolvent for the hydrophobic block, which is later removed from the solutions containing amphiphilic BCP self-assembled nanoparticles by dialysis or distillation. After removal of the organic solvent, due to strong incompatibility of the hydrophobic block with water, the self-assembly appears in a so-called “kinetically-frozen” state as activation energies for extracting a BCP chain from the self-assembly or inserting it to the self-assembly from the solution become too large and the exchange of BCP chains between the particles and the solution is stopped.

It is thus assumed that if water content in the solution is increased fast and strongly enough, the self-assembled nanoparticles keep the association number they had in the original solution before mixing with a surplus of water. This procedure, introduced by Adi Eisenberg, is referred to as quenching. Interestingly, a similar technique called nanoprecipitation or solvent displacement (that is, fast mixing of polymer solution in mild selective solvent with a surplus of a precipitant of the polymer) has been used for preparation of nanoparticles from hydrophobic homopolymers dispersed in water. It is based on the fact that instead of macroscopic phase separation of the hydrophobic polymer after mixing with water, the polymer precipitates in the form of nanoparticles which are basically microscopic phase domains of the separated polymer. In such a case, however, the size of the particles is controlled kinetically unlike that thermodynamically controlled self-assembly of BCPs in selective solvents before quenching. In practice, however, quenching is always imperfect and BCP micelles may undergo secondary aggregation which is kinetically controlled.

In this thesis, we used quenching/nanoprecipitation for preparation of aqueous dispersion of two amphiphilic star copolymers with hydrophilic arms of poly(N,N-dimethylaminoethyl methacrylate) (PDMAEMA) and hydrophobic arms of poly(lauryl methacrylate) (PLMA) differing in the length of PDMAEMA and PLMA arms. We characterized the star copolymer nanoparticles using static and dynamic light scattering and transmission electron microscopy and studied the influence of preparation conditions and solvent pH and ionic strength on size and molecular weight of the nanoparticles to gain insight on association behavior of amphiphilic star copolymers in selective solvents.



## 2. Overview of literature

### 2.1. Block copolymers

Copolymers are polymeric materials consisting of two or more chemically different monomer types in the same chain joined by covalent bonds. Block copolymers, BCPs, are defined as polymer structures with two or more chemically different monomer units, which are clustered in blocks of the polymer chains linked via their reactive ends. Properties of block copolymers can vary, depending on compatibility of each type of the constituent block with used solvent. Thanks to advanced synthetic methods and controlled polymerisation techniques along with post-polymerisation functionalization, block copolymers can be prepared with precision and controlled molecular weights and defined architectures.

### 2.2. Molecular architectures of BCPs

Block copolymers are normally prepared by controlled polymerization of one monomer followed by chain extension with different monomer to form diblock (AB), triblock (for example, ABA or ABC) or more numerous multiblock copolymers with differing structures. Molecular architectures of block copolymers can be linear, branched or cyclic structures. Under specific conditions BCPs with immiscible blocks can microphase separate and form variety of bulk morphologies which include spheres, cylinders, lamellae etc. In case of block copolymers composed of A and B repeat unit, the observed morphologies include A(B) spheres positioned on a body centred cubic lattice in a B(A) matrix, A(B) cylinders arranged on a hexagonal lattice in a B(A) matrix and coalternating lamellae. Examples of nonclassical morphologies of AB or ABA block copolymers include gyroid and lamellar morphologies.<sup>[6]</sup>

### 2.3. Star-shaped block copolymers

Star-shaped copolymers are a defined group of macromolecular architectures consisting of several linear branches, arms, attached to a single branching point, called the core. To be defined as star-shaped copolymer, at least three chains have to radiate from the multifunctional centre. The number of arms can vary from a few to tens of branches. Based on the chemical structure, monomer composition and sequence, molecular weight

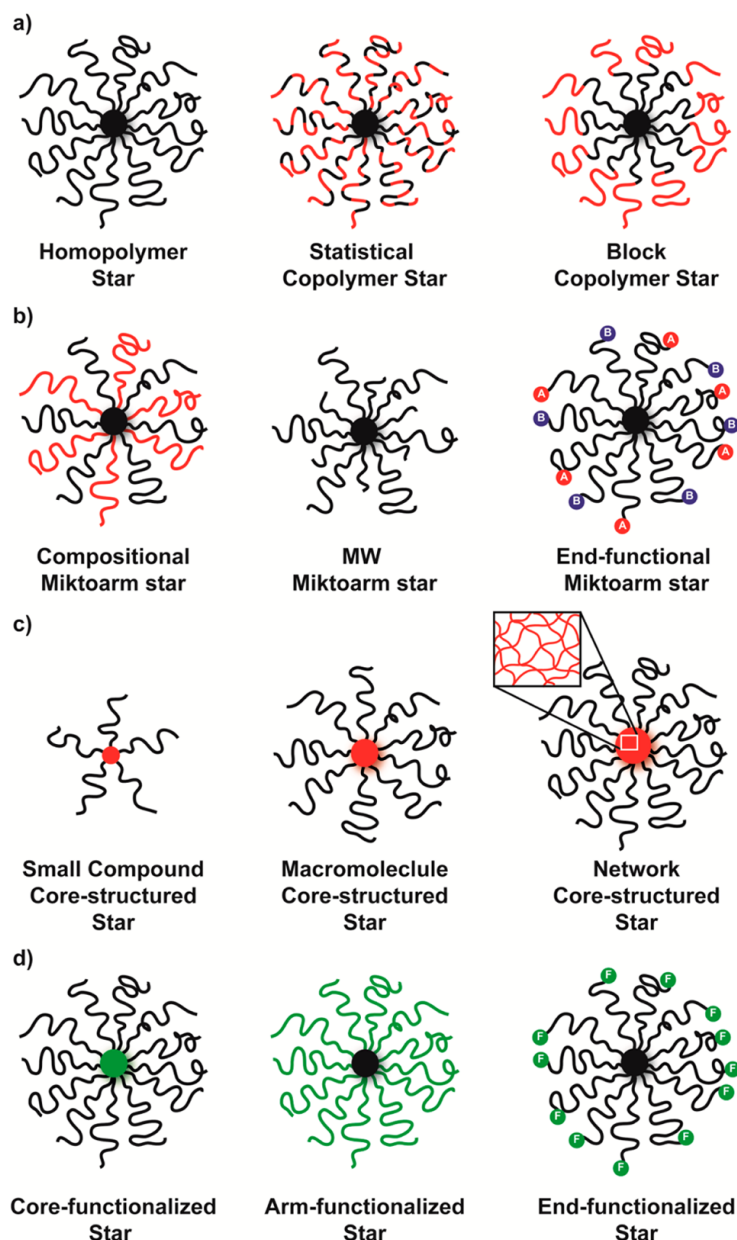


Figure 1 - Classification of star BCPs by (a) sequence distribution of the arm polymer and composition, (b) difference in arm functional groups and composition, (c) core structure, (d) functional placement [8]

distribution and many other factors, star polymers can be further classified into various categories as shown in Figure 1. Homoarm star copolymers contain symmetrical arms with similar molecular weight and matching chemical composition. Alternatively, heteroarm star copolymer can contain unsymmetrical arms with diverse chemical composition and different molecular weights. Structure, functionality, the number of functional groups as well as other characteristics of the core, can define the properties of the whole molecule. Star polymers have a higher segment density due to their smaller size compared to linear polymers. Thanks to the development in synthetic techniques, a wide range of this type of copolymers is available.

Living polymerisation of star BCPs are mainly categorized into three type: 1) the arm-first

approach, 2) the core-first approach and 3) the in-out approach. Each of the mentioned approaches has certain advantages and disadvantages.

#### 2.4. Living polymerisations of star-shaped macromolecules

The method of multifunctional initiators also referred to as the controlled core-first polymerisation is dependent of a premade multifunctional macromolecule or a well-defined initiator from which arms are grown. A low molecular weight initiator with multiple functional groups allows for the synthesis of a star block copolymer with well-defined number of arms. Number of initiating sites of the core determines the number of arms attached. To achieve best results in this approach, all initiating sites on the core should have equal reactivity and maximum initiation efficiency. By using a hyperbranched core with high molecular weight, less well-defined star copolymers are prepared. Benefits of this technique are numerous, such as high yields and products of highly controlled chemical composition, structure and functionality. On the other hand, the best results can be achieved with only a small molecular weight cores and limited number of arms of the star-block copolymers.

The method of multifunctional linking agents or arm-first synthesis is further divided into three main categories which include: 1) the macroinitiator approach, 2) the macromonomer approach and 3) the self-assembly cross-linking approach. The most reliable arm-first approach stems in the formation of linear functional polymers, arms, by living polymerization which are coupled to form a star. The macroinitiator approach is based on coupling monofunctional living polymeric arms with difunctional reagent. This process creates the core of the star block copolymer onto which arms are formed by chain extension of linear macroinitiator with a cross-linker. A similar approach is used in the macromonomer arm-first synthesis in which the cross-linking polymerization is initiated by a small molecule initiator, and the arm polymers are used as macromonomers. In the self-assembly cross-linking method the star polymers are prepared by connecting the arm copolymers through the cross-linkable block via the reaction of the pendant group with the di(or higher)-functional compound. Benefits of the arm-first approach can be well-defined star copolymers as control over number of arms by controlling the functionality of the linking agents. Long preparation times and the need of separation processes to gain pure star BCPs are limiting this method.

The in-out method is a combination of the aforementioned synthetic techniques. A living macroinitiator initiates the polymerization of cross-linking agents and creates a homoarm star onto which a pre-synthesized chemically different homopolymeric arms can be attached by post-polymerization modifications. Number of arms of the star BCP formed by this method is determined by number of functional groups of the cores. However only two types of polymer arms can be attached using this technique.

## 2.5. Self-assembly of star-shaped block copolymers

A large number of polymer morphologies for example, graft copolymers, cyclic polymers, linear BCPs, *etc.*, can self-organize (self-assemble) into aggregates under certain conditions. In the case of star-block copolymers or miktoarm star copolymers the use of selective solvent or changes in solvent properties, can lead to molecular self-assembly and to formation of micellar structures. The association behaviour is affected by end-groups of copolymer arms and by the choice of selective solvents. For example, numerous intermolecular associations in telechelic star copolymers lead to the formation of gels. Polymer aggregates have higher stability than small molecule aggregates, as a result of their mechanical and physical properties.

The basic parameters describing the structure of macromolecular self-assembly in solution are the squared radius of gyration,  $R_G^2$  and the hydrodynamic radius  $R_H$ . While  $R_G^2$  is the average of squared distances of segments of chains forming the particle from the centre of gravity of the particle, weighted by the masses of the segments,  $R_H$  is defined as the radius of a sphere with the same diffusion coefficient as the given particles.

The self-assembly occurs above a concentration called the critical micellization concentration or CMC. Above CMC, micelles are formed and all additional surfactant unimer molecules form micelles, whilst the concentration of nonassociated chains remains the same and is equal to CMC. If amphiphilic block copolymers are dissolved at constant temperature and in selective solvent for one of the blocks, formation of BCP micelles occurs. Aggregation number is an average number of BCP copolymer chains in a micelle above CMC.

CMC can be controlled by many factors as pH, temperature, solvent properties, molecular weight, chemical composition, *etc.* On average, star copolymers have higher


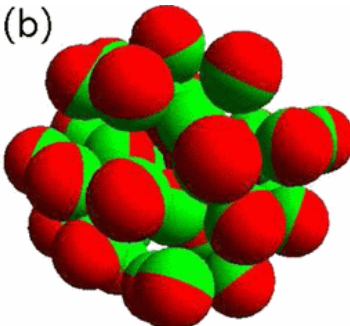
critical micellization concentrations and therefore lower aggregation numbers than comparable linear BCPs. Increasing number of arms or molecular weight of arms in star copolymers leads to a decrease in the weight average aggregation number,  $N_w$ , and also the average aggregation number,  $N_n$ . The self-assembly process is driven by an unfavorable mixing enthalpy coupled with small mixing entropy, with the covalent bond preventing macroscopic phase separation.<sup>[5]</sup>

## 2.6. Properties of BCP in solutions

Aqueous environment is very common in studies of BCP self-assembly, with respect to desired applications of BCP nanoparticles in pharmaceuticals as drug carriers. Solubility of each block of the  $A_xB_y$  copolymer in water, divides them into three categories:

1. amphiphilic, for example, block  $A_x$  is hydrophobic and block  $B_x$  is hydrophilic,
2. double hydrophilic
3. double hydrophobic

The amphiphilic star-shaped copolymers could change their conformation with solvent polarity. In a strongly selective solvent, miktoarm stars form micelles consisting of the core of soluble arms and the corona of the insoluble arms similarly to linear BCPs. In common solvents, hydrophilic chains swell. On the contrary, hydrophobic segments swell in less polar solvents. Symmetric star polymers have different solution behaviours than star

(a)  (b) 

copolymers with chains of varying molecular weight or chemical structure. In a good solvent, the increase in molecular dimensions is expected in star polymers due to higher number of hetero-

interactions between arms. It has been observed that, experimentally

found hydrodynamic radius,  $R_H$ , values of miktoarm-star copolymers are higher due to repulsive interactions between chemically different arms A and B, when these arms are

linked to the same point. This expansion occurs in star-shaped copolymers in both good and selective solvents.<sup>[9,19]</sup>

Morphologies of star-shaped block copolymers differ in polymer solutions, in bulk and in thin layers, created at surfaces and interfaces. Experiments have shown that star-shaped heteroarm diblock copolymers, in good solvent for both blocks, could form ‘‘Janus’’-like conformation. This effect is caused by slight difference in affinity to the solution between block A and block B and leads to intramolecular segregation. After forming these structures, depending on solvent properties, the ‘‘Janus’’-like molecules could create micelles or vesicles. This changes when the affinity to the solution of both blocks is nearly equal. Spherical molecules are formed.

Experiments including  $(BA)_n$  star-shaped diblock copolymer, in selective solvent for  $A_x$  block where,  $B_y$  block is situated near the centre of the molecule, indicate that due to the solvophobic qualities of B-blocks these segments attract each other and form a core to minimize contact with solvent. On the other hand, A-blocks are solvophilic and create a corona surrounding this core. For a  $(BA)_n$  star-shaped copolymer system, with high number of particles,  $n$ , there is lower chance of multimolecular micelle formation due to repulsions between individual star coronas formed by  $A_x$  block. If  $n$  is small, chance of micelle formation is higher by reason of insufficient shielding of the B-block cores, resulting to cores collapsing into each other. This process is comparable to the self-assembly of micelles from linear diblock copolymers. The difference between micelle formation from linear copolymers and star-shaped copolymers is that, if  $n$  is high enough, micelles will be unimolecular.<sup>[19,20]</sup>

## 2.7. PDMAEMA-*b*-PLMA copolymers

PDMAEMA-*b*-PLMA, poly(dimethylaminoethyl methacrylate)-*b*-poly(lauryl methacrylate) belongs to amphiphilic block copolymers able to form micelles with the PLMA hydrophobic core and the PDMAEMA hydrophilic corona in aqueous solutions. PDMAEMA is not only a hydrophilic polymer but it is also a weak polyelectrolyte (PE) as dimethylamino groups are weak bases ( $pK_b = 8,44$ ) which at neutral and low pH become protonated, forming cationic dimethylammonium groups. The transition from neutral to the charged state has strong impact on PE conformation behaviour, as electrostatic repulsion

between identical charges, leads to stretching of the PE chain. BCP self-assemblies with PE coronas are thus strongly responsive to pH. Another factor affecting the behavior of BCPs is ionic strength of the solution. Soluble salts screen Coulombic interactions in solution and thus weaken electrostatic repulsion between the charged groups along the PE chain.

Studies thus not surprisingly confirmed that PDMAEMA-*b*-PLMA copolymers responded to pH changes. The hydrodynamic radius of PDMAEMA-*b*-PLMA nanoparticles decreased with decreasing pH due to increased solubility of protonated PDMAEMA chains. At acidic pH, the copolymer was highly soluble in water which leads to disaggregation of the supramolecular structures formed at neutral pH, due to stretching of corona chains which disrupted the PLMA core. At basic pH, the PDMAEMA block was fully deprotonated and repulsive forces between arms are reduced. As a consequence, the copolymer became more hydrophobic, and formation of larger aggregates was observed.<sup>[21,24]</sup>

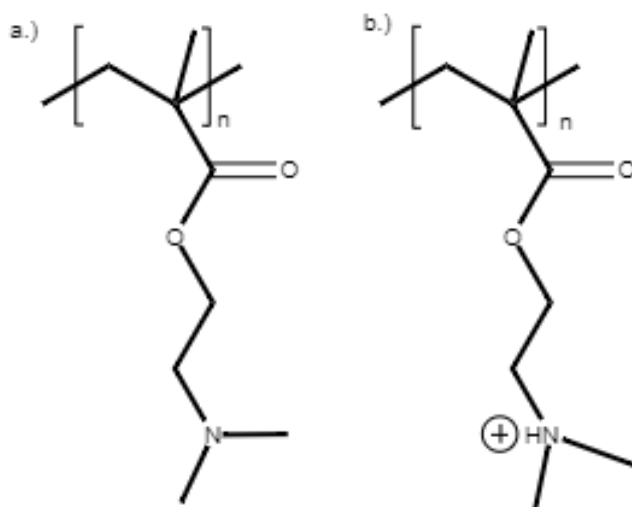


Figure 3 – Chemical structure of a.) PDMAEMA, b.) PDMAEMA with protonated cationic dimethylammonium group

## 2.8. Light scattering

Elastic scattering of electromagnetic (EMG) radiation is an interaction of the EMG wave with matter leading to a change of the wave vector while the frequency of the radiation does not change. Electromagnetic wave distorts electron distribution in the particle, which results in polarization of the molecule and creation of an oscillating dipole. This dipole can be considered as a source of scattered light and has same wavelength,  $\lambda$ , as the incident EMG wave. Light is emitted from this oscillating dipole in perpendicular directions isotropically.<sup>[29]</sup> The scattering angle  $\theta$ , is an angle at which scattered light is observed, considering the direction of transmitted light. Three major parameters are considered in light

scattering experiment, which are Rayleigh ratio,  $R$ ,  $\lambda$  and  $\theta$ . The absolute scattering intensity or Rayleigh ratio, describes loss in intensity of incident light, caused not by absorption, but due to scattering, after passage through a medium. Intensity of scattered light is proportional to the second power of polarizability of observed molecule and is inversely proportional to the fourth power of wavelength. This is applicable to particles with size from  $1/20$  of the incident light wavelength or smaller.<sup>[29]</sup> Several oscillating electric dipoles are created in molecules with size comparable to wavelength. This effect is greater with larger particles. Light emitted by these dipoles in different points in molecule is out of phase and thus scattering intensity is a superposition of waves in a point and angle of observation. In this case, light scattering is angle dependent and differences in phase are minor at small  $\theta$ .<sup>[29]</sup> An interference pattern of the scattered light, particle form factor  $P(\theta)$ , defines size and shape of individual molecules. Brownian motion of particles in solution instigates random temporal changes in local concentration of scattering particles. This phenomenon leads to changes in interferences between oscillating dipoles in molecules and shift in scattered light intensity at certain angle at time. Mobility of molecules in solution can be determined by observation of this effect, which is the basic principle of dynamic light scattering. Common methods of light scattering analysis are static light scattering (SLS) and dynamic light scattering (DLS).

In SLS, light is scattered with variable intensity at all angles when measured parallel to scattering plane. Analysis of particles larger than  $1/20$  of  $\lambda$  in solutions, the intensity of scattered light is a function of scattering angle  $\theta$ . The scattering vector  $\vec{q}$  defines quantitative measure for length scale of the SLS experiment. The value of  $\vec{q}$  is determined by the difference of wave vectors of incident light,  $\vec{k}_0$  and scattered light,  $\vec{k}$ , at observed scattering angle  $\theta$ :

$$\vec{q} = \vec{k} - \vec{k}_0 \quad (1)$$

The magnitude of scattering vector  $q$  for SLS of molecules larger than  $1/20$  of  $\lambda$  and given scattering geometry, where  $|k - k_0| = 2 \sin \theta/2$  and  $q = a \cdot |k - k_0|$  and  $a = \frac{2\pi}{\lambda}$  can be given as:

$$q = \frac{4\pi n}{\lambda_i} \cdot \sin \theta/2 \quad (2)$$



where  $\lambda$  is substituted for  $\frac{\lambda_i}{n}$ , based on the dependence of incident light wavelength  $\lambda_i$  on refractive index of solvent,  $n$ . Determining size and shape of molecule larger than  $1/20$  of  $\lambda$ , noted as a function,  $P(q)$ , a particle form factor (PFF) for isotropic particles as:

$$P(q) = 1 - \frac{1}{3} R_G^2 q^2 \quad (3)$$

where  $R_G$  is the radius of gyration. Due to large number of molecules with varying sizes and molecular architectures in observed solution, PFF is determined as an orientational average. The Zimm equation, used to create the Zimm plot, determines the relation between normalized scattered intensity  $R$  and particle form factor  $P(q)$ . It takes into account solute concentration  $c$ , interactions between solvent and solute and  $q$ . Used in light scattering analysis for particles smaller than 50 nm:

$$\frac{Kc}{R} = \frac{1}{MP(q)} + 2A_2c \quad (4)$$

where  $2A_2c$  determines the attractive/repulsive interactions between solute and solvent and,  $A_2$  is the second virial coefficient of solution osmotic pressure which provides quantitative measure for these interactions. The scattering power of individual solute particle,  $K$ , or so-called contrast factor is dependent on refractive index increment  $\frac{dn}{dc}$ , which needs to be determined to evaluate the sample. The  $K$  constant is calculated as:

$$K = \frac{(2\pi n_0)^2 \left(\frac{dn}{dc}\right)^2}{N_A \lambda^4} \quad (5)$$

where,  $n_0$ , is the refractive index of pure solvent,  $\lambda$ , is the wavelength of incident light and  $N_A$  is the Avogadro's number.  $\frac{dn}{dc}$  defines changes in refractive index with varying concentrations and can be determined by measurements of solutions of different concentrations with the same solute. For small values of  $qR$  or small  $\theta$ , the Guinier approximation of PFF is used as:

$$P(q) \approx \exp\left(\frac{-q^2 R_G^2}{3}\right) \quad (6)$$

Natural logarithm of the simplified equation (4), with substituted Guinier approximation of particle form factor, yields the function of Guinier plot, where  $\ln(R(q))$  is plotted vs  $q^2$ , for  $R$  measured at different  $q$ -values.

$$\ln(R(q)) \approx \ln(KcM) - \frac{q^2 R_G^2}{3} \quad (7)$$

Based on this equation (7), slopes of Guinier plots determine the radius of gyration. Guinier fits are valid for values of  $qR < 1$ , more accurate results are gained using this approximation at small values. The effects of sample dispersity are best observed at near minimum values of PFF. On the other hand, most accurate measurements of  $R_G$  can be done at small scattering angles.

The principle of DLS is the measurement of temporal fluctuation of scattered light due to Brownian motion of particles. Physical dimensions of scattering molecules determine characteristic rate of motion. A time dependent correlation functions is measured by dynamic light scattering:

$$G(\tau) \equiv \langle I(t)I(t + \tau) \rangle \quad (8)$$

where  $I(t)$ , is scattering intensity at time  $t$ ,  $\tau$  is the is lag time and brackets  $\langle \rangle$  denote averaging over time,  $\tau$ , the scattering intensity at given time. A dimensionless autocorrelation function can be written as:

$$C(\tau) \equiv \frac{\langle I(t)I(t+\tau) \rangle}{\langle I(t)^2 \rangle} = [1 + \gamma[g^{(1)}(\tau)]^2] \quad (9)$$

where  $\gamma$  is a constant determined by the specific experimental setup and  $g^{(1)}(\tau)$  is the normalized first order time autocorrelation function. It may be shown for a dilute solution of monodisperse nanoparticles that  $g^{(1)}(\tau)$  is a single exponential whose time decay is determined by the translational self-diffusion coefficient of the particle  $D$  and the length of the scattering vector  $q$ <sup>[34]</sup>:

$$g^{(1)}(\tau) = \exp(-q^2 D \tau) \quad (10)$$

where  $q^2 D$  can be expressed as decay rate,  $\Gamma = q^2 D$ . Measured in DLS is the diffusion coefficient  $D$ , which describes hydrodynamic interactions between solute molecules and solvent in observed scattering solution. By experimental determining the diffusion coefficient, hydrodynamic radius  $R_H$ , can be calculated from the Stokes-Einstein equation:

$$D = \frac{kT}{6\pi\eta R_H} \quad (11)$$

where  $k$  is the Boltzman constant,  $T$  is the sample temperature and  $\eta$  is solvent viscosity. An important characteristic of analysed particles is  $\rho$ -ratio, which is defined as:

$$\rho = \frac{R_G}{R_H} \quad (12)$$

Particles with distribution of sizes and architectures can be present in sample solution rather than molecules uniform in size and shape. This leads to dispersity of examined solution. In case of polydisperse system the first order time correlation function becomes sum of exponentials. For particles larger than 10 nm the measured diffusion coefficient distribution, depends on size distribution and also scattering vector  $q$ . Common used techniques for analysis of DLS data in disperse systems are the cumulant expansion and inverse Laplace transform performed by constrained regularization algorithms such as CONTIN.

## 2.9. Transmission electron microscopy

Transmission electron microscopy (TEM) is a high resolution, imaging technique used for detailed analysis of morphological features, composition and crystallization information of observed specimen. TEM is an analogous technique to light microscopy, which is limited in resolution by wavelength of light. The use of electron beam in TEM, is advantageous in magnification power due to smaller wavelength of electrons by order of  $10^5$ . Electrons are generated by field-emission electron gun a focused into small, thin and coherent beam by condenser lenses, which exclude high angle electrons. Upon reaching the specimen, portion of the electrons is transmitted through and focused by objective lens onto a phosphor screen or charged coupled device camera. An image of the specimen is generated, where contrast indicates amount of light transmitted through the sample. Areas with higher rate of transmission appear to be lighter. The created images are monochromatic, except for analysis with the use of fluorescent screen at the end of the visualization. Electron microscopy is expensive, extremely sensitive to vibrations, and sample preparation can cause damage to the specimen. To form an image, a sufficient amount of electrons need to be transmitted, with minimum energy loss. Due to high absorption and scattering of electrons, prepared samples are 20 – 100 nm thin. However, TEM technology has wide variety of uses due to high magnification power and image quality.

### 3. Materials and methods

#### 3.1. Polymer samples

Used (poly(2-(*N,N*-dimethylamino)ethyl methacrylate)-poly(lauryl methacrylate) (PDMAEMA-PLMA) miktoarm star copolymers, were synthesized in the group of Dr. Stergios Pispas (Theoretical & Physical Chemistry Institute, Athens, Greece) by the arm first method which stemmed in crosslinking of PDMAEMA ( $M_w = 6,0 \text{ kg mol}^{-1}$ ) and PLMA ( $M_w = 4,6 \text{ kg mol}^{-1}$ ) arm by the reaction with ethylene glycol dimethacrylate. Two samples were prepared, PDMAEMA<sub>41</sub>-PLMA<sub>26</sub> ( $M_w = 377 \text{ kg mol}^{-1}$ , further referred to as Saf1) and PDMAEMA<sub>29</sub>-PLMA<sub>88</sub> ( $M_w = 610 \text{ kg mol}^{-1}$ , further referred to as Saf2); the indices denote the numbers of arms. The details on synthesis and characterization are given in ref.<sup>[37]</sup>

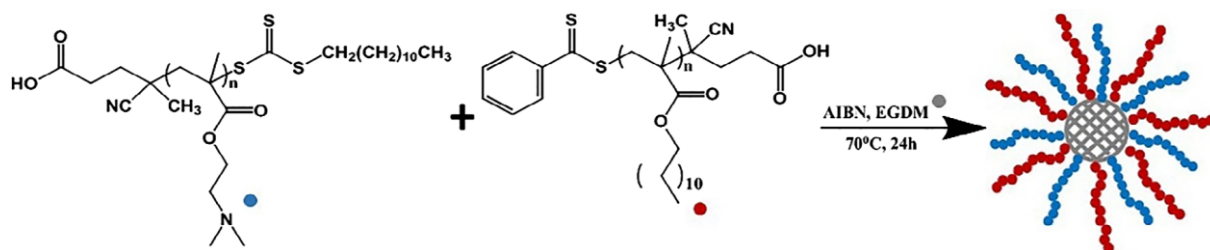


Figure 4 – Synthetic route for PDMAEMA<sub>x</sub>PLMA<sub>y</sub> amphiphilic mikto-arm stars. <sup>[37]</sup>

#### 3.2. Preparation methods

Solutions of star-shaped copolymers Saf1 and Saf2 were prepared for further analysis. As neither Saf1 nor Saf2 were directly soluble in water, THF was used as a cosolvent for dissolution in water. 5,0 mg of the polymer sample was dissolved in 0,5 ml THF/water mixture (90%/10%, v/v) and mixing with water was conducted following two protocols:

- (i) 0,5 ml of the solution in THF/water mixture was added dropwise to 4,5 ml of deionized water under vigorous stirring.
- (ii) 4,5 ml of deionized water was added dropwise to 0,5 ml of the solution in THF/water mixture under vigorous stirring.

The solutions were then extensively dialyzed against a surplus of deionized water to remove THF. In the case of Saf2, the above-mentioned procedure was modified so that water was replaced with 0,1 M HCl, 0,1 M Na<sub>2</sub>CO<sub>3</sub> and with D<sub>2</sub>O (for planned small-angle neutron

scattering measurements). The final concentration of the samples after dialysis was about 1 mg/ml. Saf2 samples were further diluted with H<sub>2</sub>O (0,1 M HCl, 0,1 M Na<sub>2</sub>CO<sub>3</sub>) prior to light scattering measurements to suppress multiple scattering. Refractive index increments  $\frac{dn}{dc}$  for individual homopolymers were obtained from literature<sup>[39,40]</sup> (the value for PLA in THF was recalculated for water using the Gladstone-Dale rule). Refractive index increments of Saf1 ( $\frac{dn}{dc} \approx 0,128$  ml/g) and Saf2 ( $\frac{dn}{dc} \approx 0,130$  ml/g) were calculated as mass-weighted average values of constituent homopolymer  $dn/dc$  with respect to copolymer compositions.

### 3.3. Photometer

The light scattering measurements were conducted on an ALV light scattering photometer (ALV, Germany), consisting of an ALV CGS3 automatic goniometer, ALV 5004 multiple tau digital correlator and a pair of high quantum efficiency avalanche photodiode (APD) detectors operated in pseudo-crosscorrelation mode. The photometer was equipped with a Cobolt Flamenco 100 mW diode-pumped solid-state laser source with the wavelength,  $\lambda = 660$  nm. The measurements were carried out in the angular range 40° –150° with the angle step 5° and at the temperature of 297 K.

### 3.4. Transmission electron microscope

Transmission electron microscopy imaging was conducted using a JEOL NeoARM microscope (JEOL, Japan) equipped with a field emission gun electron source operated at acceleration voltage 200 kV and a TemCam XF416 CMOS camera (TVIPS, Germany) with the resolution of 16 Mpix. 10 ml of the SAf2 solution in water (~1 mg/ml) was put on a 300 mesh copper grid covered with holey carbon film. After 1 min, the solution was sucked by touching the bottom of the grid with filter paper and the grid was left to dry at room temperature before it was mounted on a single tilt sample holder and inserted to the microscope.

## 4. Results and discussion

The appearances of Saf1 and Saf2 solutions after mixing with water using Protocol (i) were distinctly different: A weak bluish opalescence appeared in the Saf2 solution while no increase in turbidity was observed in the Saf1 solution which, indicated that Saf2 nanoparticles had much higher molecular weight. Such a difference can be easily explained as a consequence of Saf1 and Saf2 composition: Saf2 contains a lower number of PDMAEMA arms and thus requires association of a higher number of star macromolecules to stabilize the associate in aqueous solution.

The Saf2 solution had to be ten times diluted to suppress multiple scattering and to get scattering intensities in the range which was optimal of the APD detectors. Such a scattering behavior fully eliminated problems with dust contamination of allowed for measurements without filtration of the samples. On the other hand, weakly scattering Saf1 solutions had to be carefully filtered using membrane microfilters to obtained reliable results. Therefore, we further focused only to Saf2.

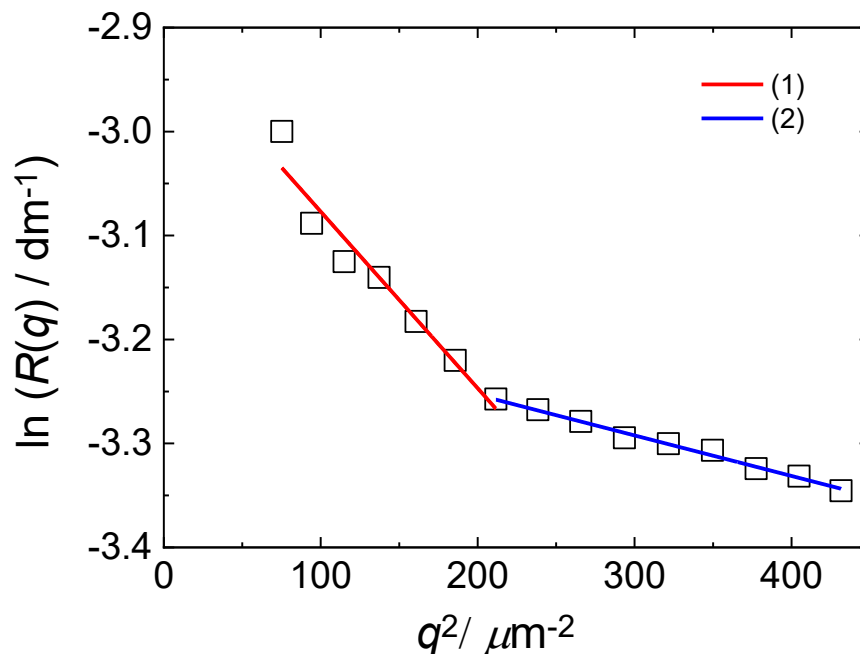


Figure 5 – Static light scattering analysis function of  $\ln(R(q))$  vs  $q^2$  of Saf1, preparation protocol (i) in pure water solution at concentration 0,930 mg/mL,

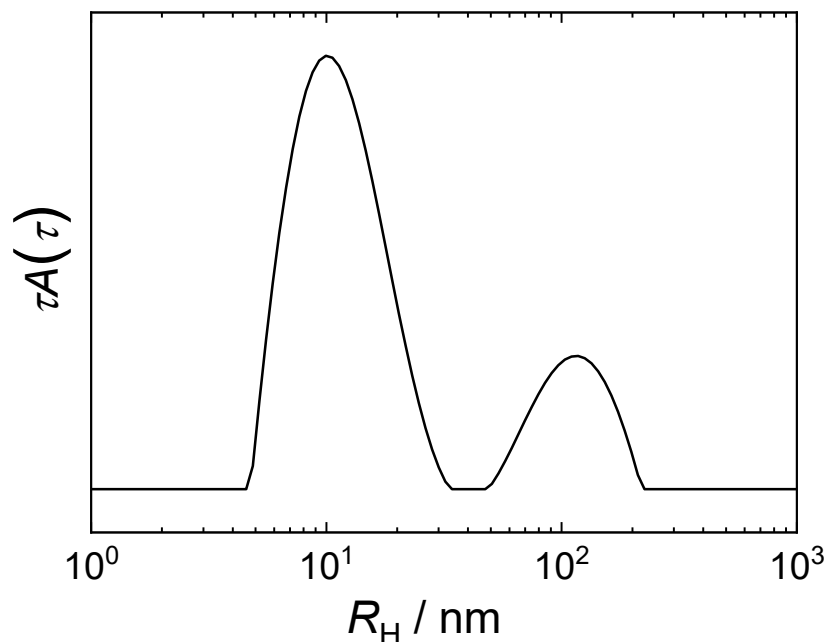


Figure 6 - Dynamic light scattering distribution function of Saf1, preparation protocol (i) in pure water solution at concentration 0,930 mg/mL

The static light scattering measurement of 0,930 mg/mL Saf1 solution prepared with the protocol (i) (Fig. 5) revealed two distinct Guinier regimes, (1) and (2), the former corresponding to the scattering from larger aggregates which dominated at lower  $q$  and the latter to the scattering from Saf1 micelles. The corresponding apparent gyration radii were  $R_{G,1} = 34$  nm and  $R_{G,2} = 71$  nm (Table 1).

The dynamic light scattering measurement (Figure 6) showed bimodal distributions of hydrodynamic radii ( $R_{H,1} = 11$  nm, and  $R_{H,2} = 110$  nm) which confirmed the coexistence of star Saf1 micelles with Saf1 larger aggregates. Assuming that the mass fraction of the Saf1 in larger aggregates is negligible, we can take the mass concentration of Saf1 for the calculation of the molar mass of the micelles,  $M_{w1} = 4,50 \cdot 10^6$  g mol<sup>-1</sup>, which corresponds to the association number of approx. 12.

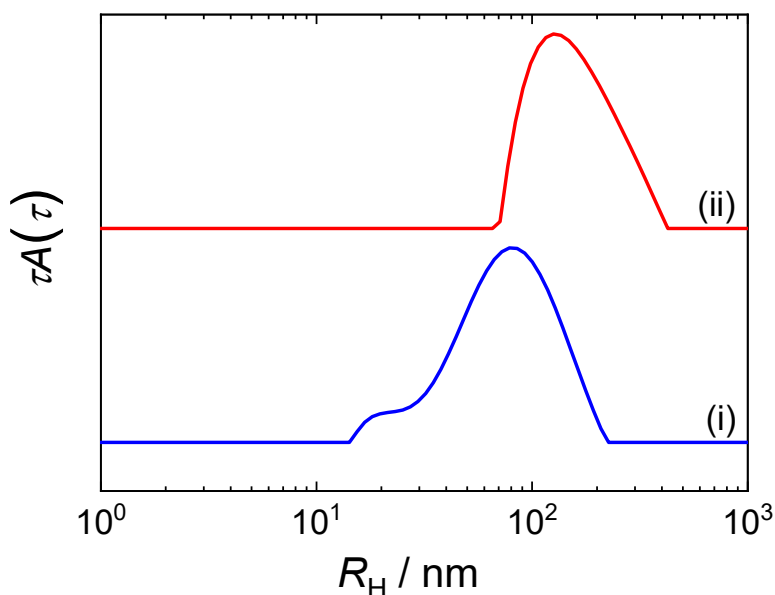


Figure 7 - DLS distribution functions hydrodynamic radii for Saf2 solutions prepared using protocols (i) and (ii).

Table 1 – Evaluation of SLS and DLS measurements for Saf1 and Saf2 copolymer solutions

Sample	$R_G$ [nm]		$R_H$ [nm]		$M_w$ [ $10^6$ g/mol]
	(SLS)		(DLS)		
Saf1	34	71	11	110	4,50
Saf2, Protocol (i)	118		72		1417
Saf2, Protocol (ii)	166		153		8269

In the case of Saf2, we used two protocols for preparation of aqueous solutions which differed in the order of mixing (In Protocol (i) Saf2 solution in THF/water is dropwise added to a surplus of water while in Protocol (ii) the procedure is reverse). The results are summarized in Table 1; Figures 8 and 9 show the distributions of hydrodynamic radii and Guinier plot for the  $q^2$  range from 70 to 240  $\mu\text{m}^{-2}$  which was used to evaluate  $R_G$ . Both SLS and DLS showed that Protocol (ii) yielded nanoparticles which were larger and had higher molar mass.

This difference can be explained as follows: When using Protocol (i), Saf2 solution in THF/water mixture is added into a surplus of water so that the solvent quality decreases instantaneously, Saf2 aggregates formed in THF/water mixture become “kinetically-frozen” and no further rearrangement is possible. Using Protocol (ii), solvent quality is being decreased gradually and so is the solubility of Saf2 in THF/water mixture. During this



process, Saf2 is in a mild selective solvent so that the sorption of Saf2 star polymers to the aggregates and the growth of the aggregates due to worsening of solvent quality can occur.

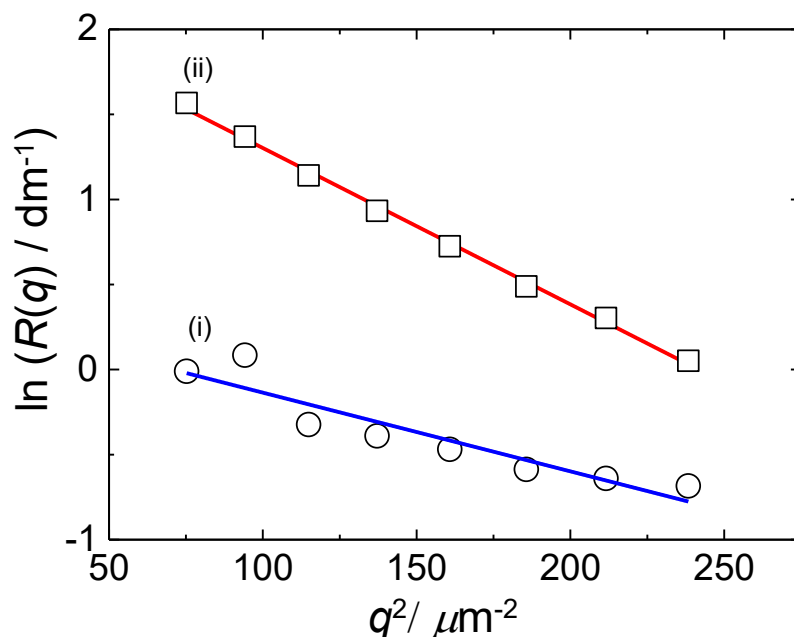


Figure 8 - SLS analysis function of  $\ln(R(q))$  vs  $q^2$  of Saf2, in pure water solution, preparation protocol (i) and (ii)

In order to demonstrate that Saf2 aggregates are kinetically frozen, we measured DLS in 0.1M HCl (pH 1,35) and 0.1 M  $\text{Na}_2\text{CO}_3$  (pH 13,3) to observe changes in the hydrodynamic radius of Saf2 aggregates caused by changes in PDMAEMA degree of protonation. While in pure aqueous solution (pH 6,82), PDMAEMA is weakly protonated, at pH 13 it becomes fully deprotonated and at pH 1 fully protonated. However, DLS measurements (Figure 9) did not reveal any swelling of the particles due to stretching of protonated PDMAEMA chains ( $R_H$  of 71 nm at pH = 1,35, is similar to 72 nm at pH = 6,82; deprotonated Saf2 at pH = 13, exhibited even a slightly larger  $R_H$  of 79 nm). Such a behavior indicates that most PDMAEMA arms are buried in the aggregates and thereby not exposed to water; changes in the surface layer are too small to affect the overall hydrodynamic size of the aggregates.

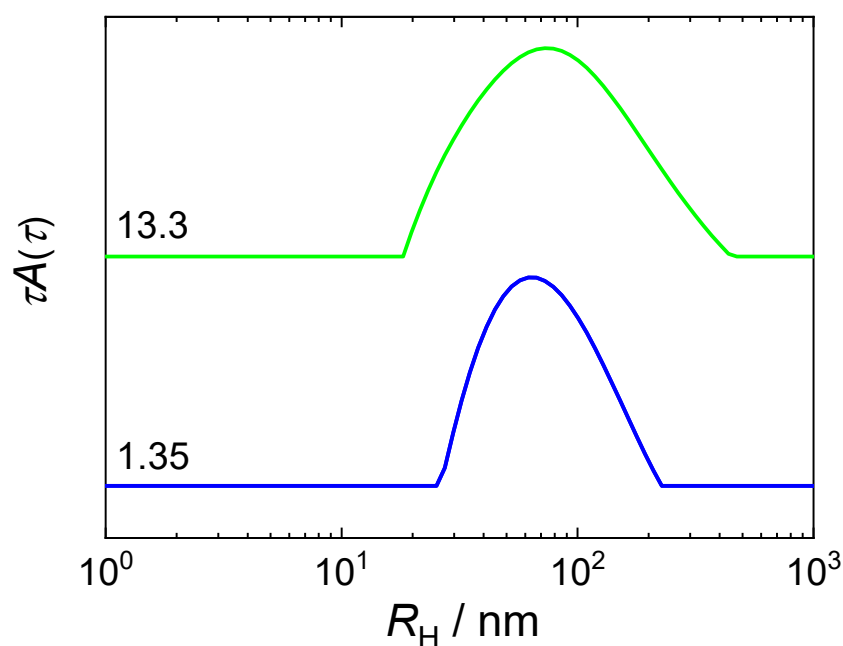


Figure 9 - DLS distribution functions hydrodynamic radii for Saf2 solutions prepared using protocol (i), with varying pH

In order to obtain deeper insight on the morphology of Saf2 aggregates, we used TEM imaging. The TEM micrograph of Saf2 aggregates (prepared with Protocol (i)) deposited on a carbon film under high vacuum conditions is shown in Fig. 10. The size of the spherical aggregates agrees with the results of light scattering measurements; the histogram of particle radii obtained from the image analysis of Fig.10 is shown in Fig. 11.

It is noteworthy that many particles on the micrograph are interconnected and form clusters. Such a behavior is not uncommon for nanoprecipitated polymer nanoparticles are often less effectively stabilized as compared with core/shell block copolymer nanoparticles. Similar structures were observed for example in aqueous solutions of polystyrene-grafted cellulose.<sup>[41]</sup>

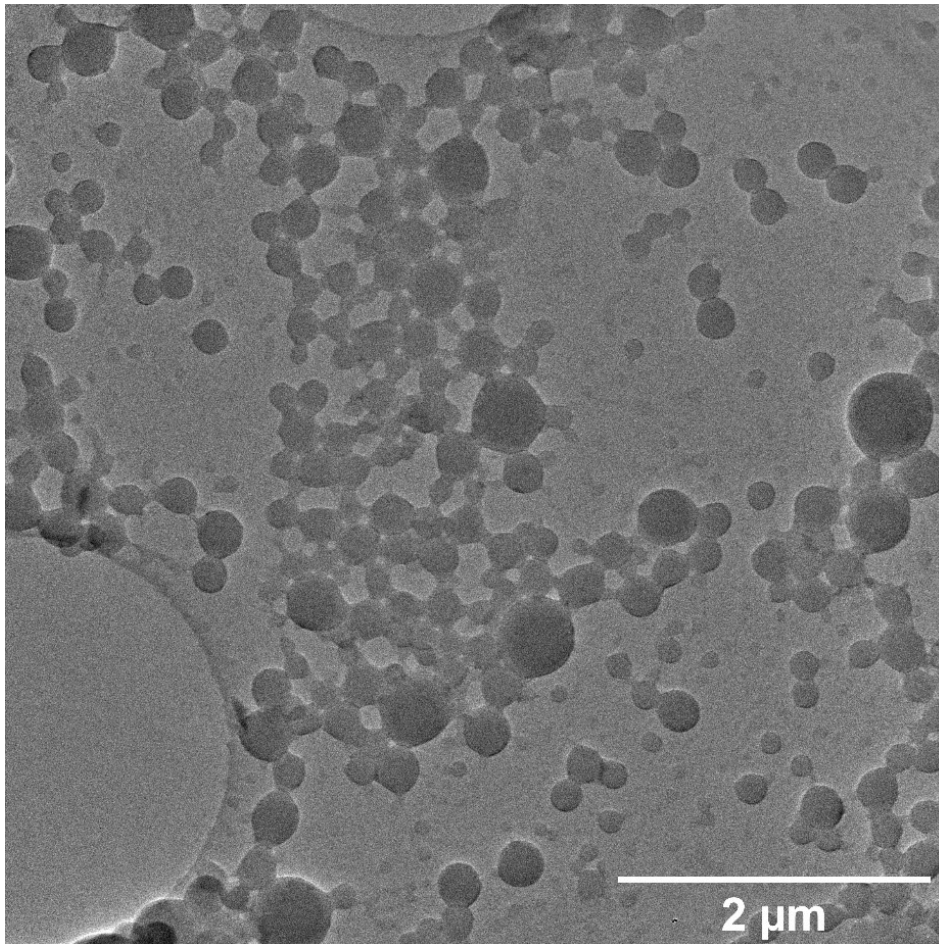


Figure 10 - TEM micrograph of Saf2 nanoparticles, prepared with protocol (i)

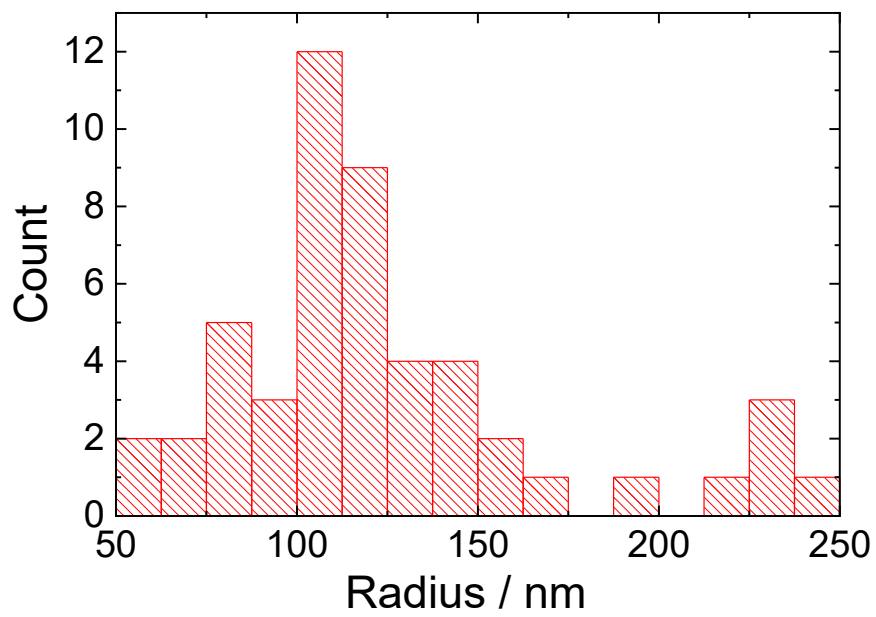


Figure 11 - Distribution of Saf2 particle radii obtained from image analysis of the micrograph in Fig. 10

## 5. Conclusion

We studied association behaviour of two miktoarm star polymers containing poly(2-(*N,N*-dimethylamino)ethyl methacrylate (PDMAEMA) and poly(lauryl methacrylate) (PLMA) arms, PDMAEMA<sub>41</sub>-PLMA<sub>26</sub> and PDMAEMA<sub>29</sub>-PLMA<sub>88</sub> (the indices denote the number of arms), in aqueous solutions. Since the samples were not directly soluble in water, aqueous solutions were prepared by the quenching technique using tetrahydrofuran (a good solvent for hydrophobic PLMA) as a cosolvent removed by dialysis against water. Characterization of the associates by static and dynamic light scattering showed that while the more hydrophilic PDMAEMA<sub>41</sub>-PLMA<sub>26</sub> formed small core/shell micelles ( $R_H = \sim 10$  nm,  $M_w = \sim 4,5 \cdot 10^6$  g mol<sup>-1</sup>), the quenching of PDMAEMA<sub>29</sub>-PLMA<sub>88</sub> yielded large aggregates ( $R_H = \sim 70$  nm,  $M_w = \sim 1,4 \cdot 10^9$  g mol<sup>-1</sup>) which, despite the presence of a weak polycation PDMAEMA, did not show any response to changes of pH. TEM imaging revealed clustering of the aggregates. From our measurements we can conclude that amphiphilic miktoarm star copolymers in which the number of hydrophobic arms is much higher than that of hydrophilic arms are not able to achieve stabilization in aqueous solutions as core/shell micelles and their association leads to the formation of nanoprecipitated aggregates, the size of which is controlled kinetically rather than by the lengths of the arms.

## 6. References

- [1]. Feng, H., Lu, X., Wang, W., Kang, N.-G., & Mays, J. (2017). Block Copolymers: Synthesis, Self-Assembly, and Applications. *Polymers*, 9(12), 494. DOI: 10.3390/polym9100494
- [2]. Ryan, A.J., Mai, S., Fairclough, P.A., Hamley, I.W., (2000). Structures of amphiphilic block copolymers in their liquid and solid states. In P. Alexandris, B. Lindman (Eds). *Amphiphilic block copolymers: Self-assembly and Applications* (pp. 151-167). Amsterdam: Elsevier.
- [3]. Abetz, V., Simon, P.F.W. (2005). Phase Behaviour and Morphologies of Block Copolymers. *Adv. Polym. Sci.*, 189, 125–212. DOI: 10.1007/b137234
- [4]. Matyjaszewski Polymer Group. (2020). Synthesis of Well Defined Macromolecules: Block copolymers. Retrieved from

- [https://www.cmu.edu/maty/materials/Synthesis\\_of\\_well\\_defined\\_macromolecules/block-copolymers.html](https://www.cmu.edu/maty/materials/Synthesis_of_well_defined_macromolecules/block-copolymers.html)
- [5]. Mai, Y., Eisenberg, A. (2012). Self-assembly of block copolymers. *Chem. Soc. Rev.*, 41, 5969–5985. DOI: 10.1039/c2cs35115c
- [6]. Spontak, R.J., Patel, N.P. (2004). Phase Behaviour of Block Copolymer Blends. In I.W., Hamley (Ed.). *Developments in Block Copolymer Science and Technology* (pp. 159-212). Chichester: JOHN WILEY & SONS, LTD
- [7]. Matyjaszewski Polymer Group. (2020). Molecules with Specific Architecture: Star copolymers. Retrieved from [https://www.cmu.edu/maty/materials/Polymers\\_with\\_Specific\\_Architecture/star-copolymers.html](https://www.cmu.edu/maty/materials/Polymers_with_Specific_Architecture/star-copolymers.html)
- [8]. Ren, J.M., et al. (2016). Star Polymers. *Chem. Rev.*, 116, 6743–6836. DOI: 10.1021/acs.chemrev.6b00008
- [9]. Hadjichristidis, N., et al. (2012). Polymers with Star-Related Structures: Synthesis, Properties, and Applications. *Polymer Science: A Comprehensive Reference*, 6, 29–111, doi:10.1016/B978-0-444-53349-4.00161-8
- [10]. Hadjichristidis, N., Pispas, S., Floudas, G. (2003). *Block Copolymers: Synthetic Strategies, Physical Properties, and Applications*. New Jersey: JOHN WILEY & SONS, LTD
- [11]. Khanna, K., Varshney, S., Kakkar, A. (2010). Miktoarm star polymers: advances in synthesis, self-assembly, and applications. *Polym. Chem.*, 1, 1171–1185. DOI: 10.1039/c0py00082e
- [12]. Hamley, I.W. (1998). *The Physics of Block Copolymers*. New York: Oxford University Press
- [13]. McNaught, A.D., Wilkinson, A. (1997). *Compendium of Chemical Terminology*. (2<sup>nd</sup> ed.). Oxford: Blackwell Scientific Publications
- [14]. Moroi, Y. (1992). *Micelles: Theoretical and applied aspects*. New York: Springer Science+Business Media
- [15]. Sun, J.T., Hong, C.Y., Pan, C.Y. (2012). Formation of the block copolymer aggregates via polymerization-induced self-assembly and reorganization. *Soft Matter*, 8, 7753-7767. DOI: 10.1039/c2sm25537e

- [16]. Kim, J.K., Yang, S.Y., Lee, Y., Kim, Y. (2010). Functional nanomaterials based on block copolymer self-assembly. *Progress in Polymer Science*, 35, 1325–1349. DOI: 10.1016/j.progpolymsci.2010.06.002
- [17]. Lapienis, G. (2009). Star-shaped polymers having PEO arms. *Progress in Polymer Science*, 34, 852–892. DOI: 10.1016/j.progpolymsci.2009.04.006
- [18]. Gohy, J.F. (2005). Block Copolymer Micelles. *Adv. Polym. Sci.*, 190, 65-136. DOI: 10.1007/12\_048
- [19]. Sheng, Y.J., Nung, C.H., Tsao, H.K. (2006). Morphologies of Star-Block Copolymers in Dilute Solutions. *J. Phys. Chem. B*, 110 (43), 21643-21650. DOI: 10.1021/jp0642950
- [20]. Scioritino, F., Giacometti, A., Pastore, G. (2009). Phase Diagram of Janus Particles. *Physical Review Letters*, 103, 237801-237804. DOI: 10.1103/PhysRevLett.103.237801
- [21]. Chrysostomou, V., Pispas, S. (2017). Stimuli-responsive amphiphilic PDMAEMA-*b*-PLMA copolymers and their cationic and zwitterionic analogs. *Journal of Polymer Science Part A: Polymer Chemistry*, 56(6), 598-610. Retrieved from <https://doi.org/10.1002/pola.28931>
- [22]. Chen, H., et al. (2020). Effects of Copolymer Composition and Subphase pH/Temperature on the Interfacial Aggregation Behavior of Poly(2-(dimethylamino)ethyl methacrylate)-block-poly(lauryl methacrylate). *J. Phys. Chem*, 124, 4563–4570. Retrieved from <https://dx.doi.org/10.1021/acs.jpcc.9b10673>
- [23]. Chen, H., et al. (2021). Effects of Ionic Strength and Ion Specificity on the Interface Behavior of Poly(dimethylaminoethyl methacrylate)-Poly(laurylmethacrylate). *Langmuir*, 37, 2419–2425. Retrieved from <https://dx.doi.org/10.1021/acs.langmuir.0c03424>
- [24]. Chountoulesi, M., et al. (2019). Stimuli-Responsive Lyotropic Liquid Crystalline Nanosystems with Incorporated Poly(2-Dimethylamino Ethyl Methacrylate)-*b*-Poly(Lauryl Methacrylate) Amphiphilic Block Copolymer. *Polymers (Basel)*, 11(9), 1400. Retrieved from <https://www.ncbi.nlm.nih.gov/pmc/articles/PMC6780812/>
- [25]. Bekhradnia, S., et al. (2015). Charged Star Diblock Copolymers in Dilute Solutions: Synthesis, Structure, and Chain Conformations. *Macromolecules*, 48, 2637–2646. DOI: 10.1021/ma502488u
- [26]. Chu, B. (1991). *Laser Light Scattering: Basic Principles and Practice* (2<sup>nd</sup> ed.). San Diego: Academic Press, Inc.

- [27]. Sun, S.F. (2004). *Physical Chemistry of Macromolecules: Basic Principles and Issues* (2<sup>nd</sup> ed.). New Jersey: JOHN WILEY & SONS, LTD
- [28]. Debye, P. (1944). Light Scattering in Solutions. *Journal of Applied Physics*, 15, 338-342. Retrieved from <https://doi.org/10.1063/1.1707436>
- [29]. Schartl, W. (2007). *Light Scattering from Polymer Solutions and Nanoparticle Dispersions*. New York: Springer Science+Business Media
- [30]. Burchard, W. (1983). Static and dynamic light scattering from branched polymers and biopolymers. *Light Scattering from Polymers. Advances in Polymer Science*, 48, 1-124.
- [31]. Berne, B.J., Pecora, R. (1976). *Dynamic Light Scattering with Applications to Chemistry, Biology, and Physics*. New York: JOHN WILEY & SONS, LTD
- [32]. Pecora, R. (2000). Dynamic Light Scattering Measurement of Nanometer Particles in Liquids. *Journal of Nanoparticle Research*, 2, 123–131. Retrieved from <https://doi.org/10.1023/A:1010067107182>
- [33]. TCI EUROPE N.V. (2021). Compound Summary for Poly(2-(N,N-dimethylamino)ethyl methacrylate). Retrieved May 30, 2021 from <https://www.tcichemicals.com/CZ/en/p/P2556>
- [34]. Merck KGaA (2021). SigmaAldrich Compound Summary for Poly(lauryl methacrylate) solution. Retrieved May 30, 2021 from <https://www.sigmaaldrich.com/catalog/product/sial/182192?lang=en&region=CZ>
- [35]. National Center for Biotechnology Information (2021). PubChem Compound Summary for 2-(Dimethylamino)ethyl methacrylate. Retrieved May 30, 2021 from [https://pubchem.ncbi.nlm.nih.gov/compound/2-Dimethylamino\\_ethyl\\_methacrylate](https://pubchem.ncbi.nlm.nih.gov/compound/2-Dimethylamino_ethyl_methacrylate).
- [36]. Stepto, R., et al. (2015). Definitions of terms relating to individual macromolecules, macromolecular assemblies, polymer solutions, and amorphous bulk polymers (IUPAC Recommendations 2014). *Pure Appl. Chem.*, 87(1), 71-120. DOI 10.1515/pac-2013-0201
- [37]. Skandalis, A., Pispas, S. (2019). Synthesis of (AB)<sub>n</sub>-, A<sub>n</sub>B<sub>n</sub>-, and A<sub>x</sub>B<sub>y</sub>-Type amphiphilic and Double-Hydrophilic Star Copolymers by RAFT Polymerization. *Journal of Polymer Science Part A: Polymer Chemistry*, 56(16), 1771-1783. DOI: 10.1002/pola.29447

- [38]. Teper, A., et al. (2020). Antimicrobial Activity of Hybrid Nanomaterials Based on Star and Linear Polymers of *N,N'*-Dimethylaminoethyl Methacrylate with In Situ Produced Silver Nanoparticles. *Materials*, 13, 3037. DOI: 10.3390/ma13133037
- [39]. Wright, D.B., et al. (2015). Tuning the aggregation behavior of pH-responsive micelles by copolymerization. *Polym. Chem.*, 6, 2761-2768. DOI: 10.1039/c4py01782j
- [40]. Coelho, J.F.J., et al. (2007). Synthesis of Poly(lauryl acrylate) by Single-Electron Transfer/Degenerative Chain Transfer Living Radical Polymerization Catalyzed by  $\text{Na}_2\text{S}_2\text{O}_4$  in Water. *Macromol. Chem. Phys.*, 208, 1218-1227. DOI: 10.1002/macp.200700015
- [41]. Hajduová, J., et al. (2014). Structure of polymeric nanoparticles in surfactant-stabilized aqueous dispersions of high-molar-mass hydrophobic graft copolymers. *Colloids and Surfaces A: Physicochemical and Engineering Aspects*, 456, 10-17. DOI: 10.1016/J.COLSURFA.2014.04.059